

Nanoplastics in Water: Artificial Intelligence-Assisted 4D Physicochemical Characterization and Rapid In Situ Detection

Zi Wang, Devendra Pal, Abolghasem Pilechi, and Parisa A. Ariya*



Cite This: *Environ. Sci. Technol.* 2024, 58, 8919–8931



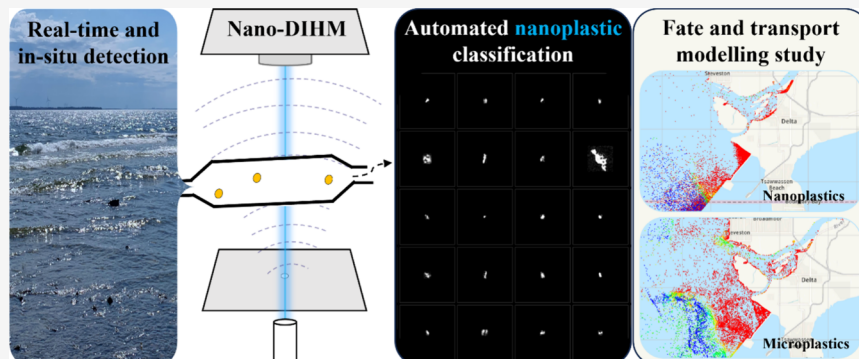
Read Online

ACCESS |

Metrics & More

Article Recommendations

Supporting Information



ABSTRACT: For the first time, we present a much-needed technology for the in situ and real-time detection of nanoplastics in aquatic systems. We show an artificial intelligence-assisted nanodigital in-line holographic microscopy (AI-assisted nano-DIHM) that automatically classifies nano- and microplastics simultaneously from nonplastic particles within milliseconds in stationary and dynamic natural waters, without sample preparation. AI-assisted nano-DIHM identifies 2 and 1% of waterborne particles as nano/microplastics in Lake Ontario and the Saint Lawrence River, respectively. Nano-DIHM provides physicochemical properties of single particles or clusters of nano/microplastics, including size, shape, optical phase, perimeter, surface area, roughness, and edge gradient. It distinguishes nano/microplastics from mixtures of organics, inorganics, biological particles, and coated heterogeneous clusters. This technology allows 4D tracking and 3D structural and spatial study of waterborne nano/microplastics. Independent transmission electron microscopy, mass spectrometry, and nanoparticle tracking analysis validates nano-DIHM data. Complementary modeling demonstrates nano- and microplastics have significantly distinct distribution patterns in water, which affect their transport and fate, rendering nano-DIHM a powerful tool for accurate nano/microplastic life-cycle analysis and hotspot remediation.

KEYWORDS: *four dimensional, real-time, in situ, nanoplastics, physicochemical characterization, deep neural network, predictive model, life cycle*

1. INTRODUCTION

Nanoplastics enter the environment through direct emissions and secondary breakdowns.¹ Microplastic degradation may generate an increased number of nanoplastic particles, by 2 to 3 orders of magnitude.² Due to their small sizes and light weights, nanoplastics possess substantial potential for extensive dispersion in natural surroundings.^{3,4} Nanoplastics exist in snow, air, polar ice, and subtropical ocean gyres.^{3,5–7} Waterborne nano/microplastics can reshape the aqueous carbon storage and contribute to global warming; while airborne nano/microplastics can alter the Earth's energy budgets and affect climate change.^{8–11}

Environmental nano- (<1 μm) and microplastics (<1 mm) have emerged as significant global concerns.^{8,12,13} Particle- and mass-based techniques allow particle imaging and chemical composition analysis of nanoplastics, like surface-enhanced Raman spectroscopy, near-edge X-ray absorption fine-structure spectroscopy, thermal-desorption proton-transfer-reaction

mass spectrometry, and so forth ([Note S1](#) and [Table S1](#)).^{3,5,14–16} Yet, there is currently no technology for in situ and real-time physicochemical processes of nano/microplastics in natural waters, precluding accurate nano/microplastic life-cycle analysis in the Earth's aquatic systems.^{8,12,13,17,18}

Nanoplastics possess distinct physicochemical characteristics compared to microplastics, which can result in disparate fates and toxicities.^{1,12} For instance, given their colloidal nature, nanoplastics are more likely to be expelled from sea ice.¹⁹ Due to their high surface-to-volume ratios, nanoplastics tend to

Received: December 11, 2023

Revised: March 3, 2024

Accepted: March 27, 2024

Published: May 6, 2024



adsorb a greater amount of other contaminants.^{20,21} Furthermore, nanoplastics likely pose more significant threats to living organisms than microplastics, as they can more easily penetrate cellular membranes.^{1,22} Understanding the characteristics, concentrations, mechanisms, and transport of nanoplastics is essential for exposure and risk studies.^{2,23} However, given the limited data, many current assessments are based on the knowledge extrapolated from microplastic or nanomaterial research, which sometimes may not be applied.^{2,24}

Numerical models play a crucial role in predicting the fate and transport of nano/microplastics, serving as one of the primary approaches for researchers and decision makers to understand the behaviors, extents, accumulation zones, and potential sources of plastic pollution.^{25,26} The capability of the models to generate reliable predictions is heavily reliant on input data quality for model initialization and boundary conditions. These include details about the concentrations and characteristics of the modeled particles like size, shape, sedimentation velocity, aggregation rate, and degradation rate.^{27,28} Such information is needed for environmental nano/microplastic life-cycle analysis, yet it is not available until this study.²⁷ We use AI-assisted nano-DIHM to acquire physicochemical data of environmental nano/microplastics and show by a modeling study the distinct transport pathways and accumulation zones of nano- and microplastic particles in waters. We address the United Nations Environment Programme tackled urgency on in situ and real-time nano/microplastic detection in aquatic systems to improve environmental assessments and targeted remediation strategies.^{29,30}

Herein, we develop a novel technology, artificial intelligence-assisted nanodigital in-line holographic microscopy (AI-assisted nano-DIHM), to fill this knowledge gap.^{28,31,32} The principle of nano-DIHM is described in **Methods** and **Note S2**. We present in the following: (1) nano-DIHM identifies nano/microplastics and other materials based on intensity and optical phase by manual reconstructions; (2) encompassing a deep neural network, AI-assisted nano-DIHM automatically characterize and classify nano- and microplastic particles in environmental waters without sample preparation; (3) the three-dimensional (3D) particle spatial/structural and four-dimensional (4D) dynamic tracking capabilities of nano-DIHM allow us to address the knowledge gap on real-time and in situ studies of waterborne nano/microplastics; (4) a model study demonstrating the distinct distributions of nano- and microplastics in the natural waters suggests that real-time nano/microplastic detection is necessary for accurate life-cycle analysis and targeted remediation. AI-assisted nano-DIHM, tailored specifically for nano- and microplastic particles, serves as a powerful tool to tackle the emerging environmental challenges posed by plastic pollution.

2. METHODS

2.1. Nanodigital In-Line Holographic Microscopy (Nano-DIHM).

In digital in-line holographic microscopy (DIHM), an interference pattern (or hologram) is formed by the interaction between a reference wave and the scattered light from the analytes/objects. The hologram is captured by a complementary metal-oxide semiconductor (CMOS)-photosensitive matrix sensor. To extract particle morphological characteristics and obtain 3D data from the recorded 2D images, numerical algorithms based on the Kirchhoff-Helmholtz transform are employed in this study.^{31,33,34}

The amplitude $A(r, t)$ and intensity $I(r, t)$ of the hologram are expressed as

$$A(r, t) = A_{\text{ref}}(r, t) + A_{\text{scat}}(r, t) \quad (1)$$

$$I(r, t) = A(r, t)A^*(r, t) \quad (2)$$

where $A_{\text{ref}}(r, t)$ is the amplitude of the reference wave and $A_{\text{scat}}(r, t)$ is the amplitude of the wave scattered by the analyte. The intensity expressed in eq 2 can be further expanded as

$$\begin{aligned} I(r, t) = & A_{\text{ref}}(r, t)A_{\text{ref}}^*(r, t) + [A_{\text{ref}}(r, t)A_{\text{scat}}^*(r, t) \\ & + A_{\text{scat}}(r, t)A_{\text{ref}}^*(r, t)] + A_{\text{scat}}(r, t)A_{\text{scat}}^*(r, t) \end{aligned} \quad (3)$$

where the first term represents the intensity of the reference waves; the second term, also known as the holographic diffraction pattern, describes the superposition of the interference between the incident reference wave and the scattered wave; the third term depicts the interference between the scattered waves, which also refers to the classical diffraction pattern.^{33,34} The amplitude of the scattered hologram is expressed as

$$A_{\text{scat}}(r) = \frac{iA_{\text{ref}}}{r\lambda} \int \int I(r) \frac{\exp(ik\frac{rr'}{r})}{|r - r'|} ds \quad (4)$$

In this work, we used a 4Deep digital in-line holographic microscope with Octopus software to record and manually reconstruct holograms. We implement an additional convolution–deconvolution route in the coding of the software to improve the resolution for detecting nanosized particles.³¹ The particle size measured from manual reconstructions is determined based on the full width at half-maximum of the peak from the intensity crosscut.³⁵ Additional information and schematic illustration of the principle of DIHM are in **Note S2** and **Figure S1**.

2.2. Detecting Nano-, Micro-, and Nonplastics using Nano-DIHM in Stationary Mode. The following suspensions are prepared: polyethylene (PE), polypropylene (PP), polystyrene (PS), polyethylene terephthalate (PET), polyvinyl chloride (PVC), and polyurethane (PUR) nanoplastic hydro-sols; suspensions of 0.05 μm polystyrene latex (PSL), microplastics, phytoplankton, magnetite, titanium dioxide, oleic acid, and humic acid; a sample of oleic acid-coated PE nanoplastics; and a mixture of PE nanoplastics, PS nanoplastics, oleic acid, magnetite, and phytoplankton. See **Note S3** for details.

Prepared suspensions are analyzed using nano-DIHM in stationary mode. For each analyte, a micropipette is used to transfer 50 μL of the suspension onto a precleaned quartz microscopic slide. Immediately, a cover slide is applied, spreading the sample into a thin film.³² For nanoplastic analysis, a thin microscopic cover slide is used in place of the conventional microscopic slide. This substitution minimizes the laser-to-sample distance, enabling improved resolution in the imaging process.³¹ For the PE pellet, the particle is directly placed onto a microscopic slide without a cover slide. The source-to-camera distance is occasionally adjusted, depending on the size of the analyte and the desired field of view. For nanoplastic samples, the source-to-camera distance is 6 mm. For oleic acid, humic acid, phytoplankton, and the mixture of nanoplastics and nonplastics, the distance is 15 mm. For all of the microplastic particles, the distance is 19 mm. The values

are 12 mm for magnetite and titanium dioxide and 20 mm for the PE pellet. Five hundred holograms of each sample are recorded at 16 fps.

Raw holograms are manually reconstructed using Octopus software. The reconstruction plane in the *z*-direction is changed frequently to bring the analyte into focus (Note S4 and Figure S2). For further comparison, 2D intensity and phase reconstruction images and particle crosscuts are acquired.

2.3. Automated Particle Characterization and Classification by AI-Assisted Nano-DIHM. Artificial intelligence (AI) is a broad field categorized into multiple subfields, such as machine learning, computer vision, and natural language processing.^{36,37} In this research, we feed the 4D Stingray software with several thousand raw holograms of nano- and microplastic particles and nonplastic river-borne (or lake-borne) particles. The objects are then found automatically by flexible analysis criteria, and more than 20 morphological parameters (e.g., particle size, shape, optical phase, perimeter, area, surface roughness, and edge gradient) of each particle are quantified and stored in our database with an assigned taxon.³⁸ Subsequently, deep neural network classifiers are trained using selected input data (i.e., images and morphological parameters) from different taxa under supervised learning, which belongs to one of the subcategories of machine learning in AI. Once the classifiers pass the validation step with >95% confidence, they are employed to automatically classify mixture samples via machine vision algorithms, an important component of computer vision systems in AI.³⁸ The classifier can be operated in real-time or offline.^{32,38} Detailed automation processes and a workflow chart are in Note S5 and Figure S3.

Autoclassification of PE nanoplastics, PS nanoplastics, oleic acid, magnetite, and phytoplankton from a suspension mixture is achieved by the following steps, PE is taken as a starting point: (1) the raw holograms of PE are recorded by nano-DIHM using Octopus software; (2) the raw holograms are loaded into Stingray software, which extracts particle images and morphological data automatically; (3) a taxon named “PE” is created and extracted particles were assigned to “PE”; (4) steps (1)–(3) are repeated for all the other analytes and “PS”, “Oleic acid”, “Magnetite”, and “Phytoplankton” taxa are created; (5) a classifier is trained with the five taxa aforementioned and the classifier is validated with objects in the database; (6) raw holograms of the mixture of PE, PS, oleic acid, magnetite, and phytoplankton are recorded by Octopus software; (7) the raw holograms are input into Stingray to extract particle images and physicochemical statistics; and (8) the validated classifier is applied to the unknown particles for autoclassification.

As the output particle size data from the software are known to be overestimated, a size correction method is adapted to adjust the raw data to actual particle size^{39,40}

$$S_{\text{corr}} = 0.121 \times S_m \times D_m^{0.76} \quad (5)$$

where S_{corr} is the corrected particle size, S_m is the autoreconstructed particle size, and D_m is the source-to-object distance measured in mm. In the experiment examining the mixture of PE nanoplastics, PS nanoplastics, oleic acid, magnetite, and phytoplankton, the source-to-object distance is 3 mm.

2.4. Detection of Waterborne Nano/Microplastics by AI-Assisted Nano-DIHM in Dynamic Mode.

Several

environmental waters are collected from two sampling sites along the Great Lakes - Saint Lawrence waterway, located at Lake Ontario in Kingston (44.2°N, 76.5°W) and Saint Lawrence River in Montreal (45.5°N, 73.5°W), Canada, in July 2022. A map of the sampling sites is in Note S6 and Figure S4. Surface waters are collected in presterilized jars while wearing gloves and a full-body clean suit. Six jars of samples are taken. Milli-Q water is used as field blanks. Multiple analyses are performed to ensure accuracy of the data accuracy.

Nano-DIHM is carried out in dynamic mode with 16 fps. A syringe pump draws the environmental waters through the system via a flow cell directly, without any sample pretreatment (Note S6 and Figure S5). The laser-to-camera distance is 1.5 cm. Recorded holograms are used for automation and 3D and 4D particle analysis. During autoreconstruction, the software scans a number of 1000 reconstruction planes for each hologram, from 1–8000 μm searching distance in the *z*-direction within the studied volume. The intensity threshold is 135 arbitrary units. Particles below 1000 μm in size are targeted.

With similar procedures shown in the previous section, a classifier consisting of “Lake Ontario” (or “Saint Lawrence River”) and “Nanoplastics” taxa is trained. The “Nanoplastics” taxon contains the input data of all six types of plastics, including PE, PP, PS, PET, PUR, and PVC (see Note S7 for more information). The classifier is applied to classify the particles in the environmental waters. Field blanks and positive controls are analyzed systematically.

2.5. 3D Particle Analysis and 4D Dynamic Tracking.

3D particle size (width, height, and length) and position data (XYZ orientations) are obtained by using the 3D reconstruction functionality of Octopus software. 3D images of individual particles within the studied volume are generated, enabling volumetric geometric analysis. The consecutive recording of the holograms at a known frame rate (16 fps) facilitates the particle dynamic tracking in a 4D (3D + time) manner, allowing us to observe and analyze the movement and behavior of particles over time.

2.6. Validation of AI-Assisted Nano-DIHM Results by Complementary Techniques.

The particle morphological observations acquired using AI-assisted nano-DIHM are validated by high-resolution transmission electron microscopy (HR-TEM) images. The detection of nano- and microplastics in environmental waters is confirmed by nanostructured laser desorption/ionization time-of-flight mass spectrometry (NALDI-TOF-MS). The particle size distribution is analyzed by utilizing an aquatic particle sizer (PSA) and a nanoparticle tracking analyzer (NTA), and the results are compared with the particle size data obtained using AI-assisted nano-DIHM. Metal and total organic carbon contents of the environmental samples are measured. Note S8 provides analysis details. Information on instruments, materials, and supplies is in Note S9.

2.7. Distinct Distributions of Nano- and Microplastics by Model.

The CaMPSim-3D numerical model simulates the transport of nanosized (800 nm) and microsized (50 μm) PET plastic particles (density = 1288 kg·m⁻³) in the Fraser River, the longest river in British Columbia, Canada (Note S10 and Figure S6). The model is developed at the National Research Council Canada and previously validated with substantial observational and real-world field measurement data.^{25,41}

CaMPSim-3D is a three-dimensional particle tracking model (PTM), relying on TELEMAC modeling system to incorpo-

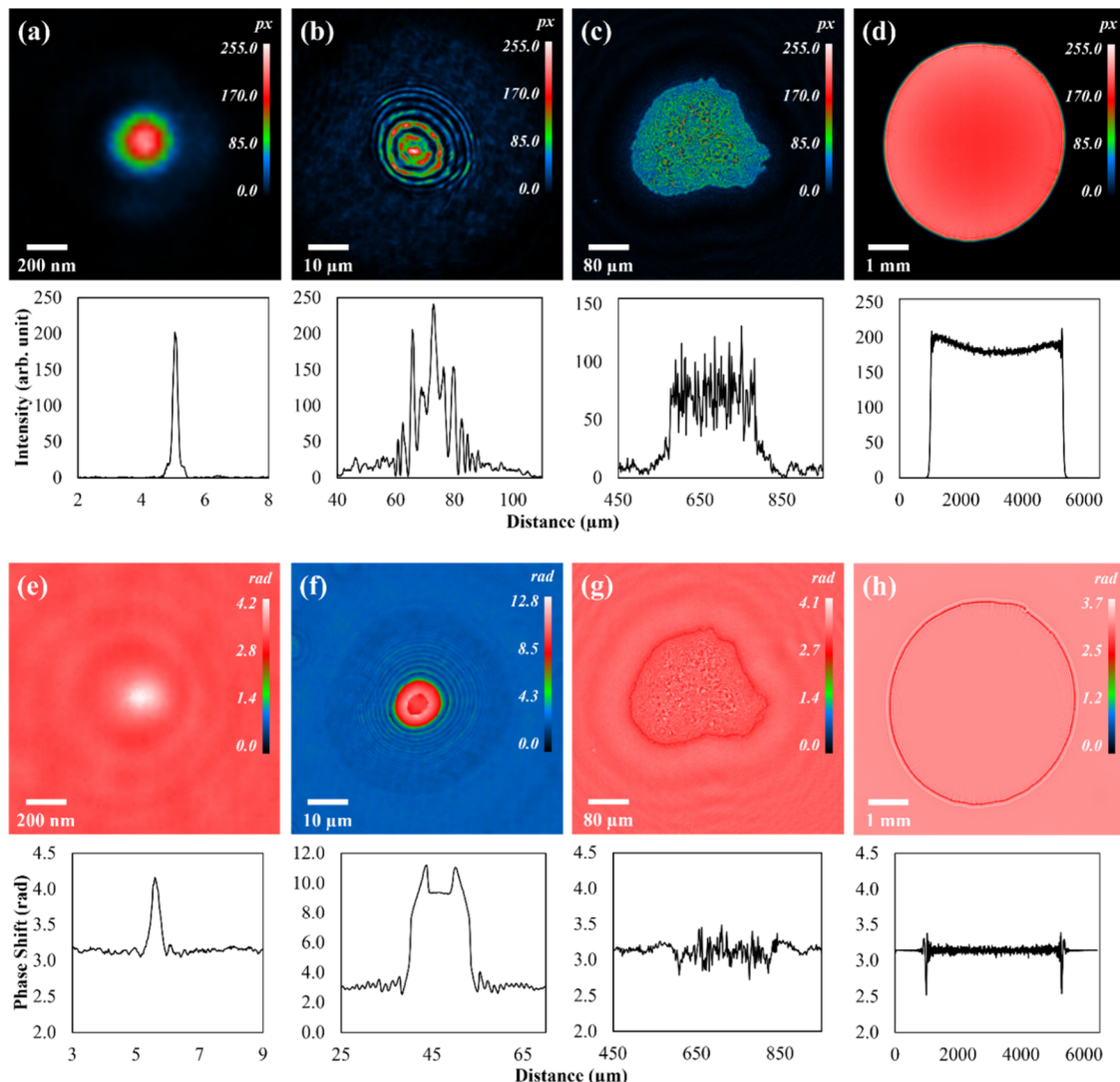


Figure 1. Intensity and phase reconstructions (images and crosscuts) of nano/micropolyethylene (PE) plastic particles in Milli-Q water. Intensity reconstructions of (a) a PE nanoplastic particle 197 nm in diameter at reconstruction plane $z = 403 \mu\text{m}$; (b) a PE nanoplastic particle coated by organic oleic acid in water at $436 \mu\text{m}$; (c) a PE microplastic particle 215 μm in width reconstructed at $6036 \mu\text{m}$; (d) a PE pellet measuring 4.5 mm at reconstruction plane $19794 \mu\text{m}$. (e–h) Phase reconstructions in respective to panels (a–d). Reconstructions are carried out manually using the 4Deep Octopus software.

rate the hydrodynamic characteristics of the studied domain.^{25,42} CaMPSim considers particles as passive objects moving at the velocity of ambient water in the horizontal direction. The horizontal component of the particle velocity is directly calculated from the hydrodynamic model. The vertical component (W_p) is calculated from eq 6, where W_w is the vertical velocity of the ambient water acquired from the hydrodynamic model, and W_s is the particle sedimentation velocity usually derived from available empirical data.

$$W_p = W_w + W_s \quad (6)$$

The hydrodynamic model is previously developed and validated using extensive topographic and oceanographic data for modeling water circulation within Fraser River between Douglas Island and Straight of Georgia.⁴¹ The model is driven by fluvial flow at the upstream boundary and a tidal current prescribed at the downstream boundary of the domain in the Straight of Georgia. It can capture the stratified flow generated by the freshwater fluvial discharge in the Fraser River as it

flows over and mixes with the saltwater intruding into the domain from the ocean.⁴¹

For both the nano- and microplastics, 10^5 particles are uniformly distributed and released at the water surface (particle elevation of 0 m) at the upstream boundary of the computational domain. The transport of these particles within the system is then simulated for 17 days. To highlight the dominant physics governing the transport, the microsized PET is modeled based on advection with a sedimentation velocity assigned based on our previous work using nano-DIHM.²⁸ For nanosized PET particles, advection and Brownian motion are considered. Once the simulation is completed, the particle distribution data is utilized in a machine learning-based clustering model to determine the potential accumulation zones of plastic pollution in aquatic systems.⁴¹ See Note S10 for more details of the modeling study.

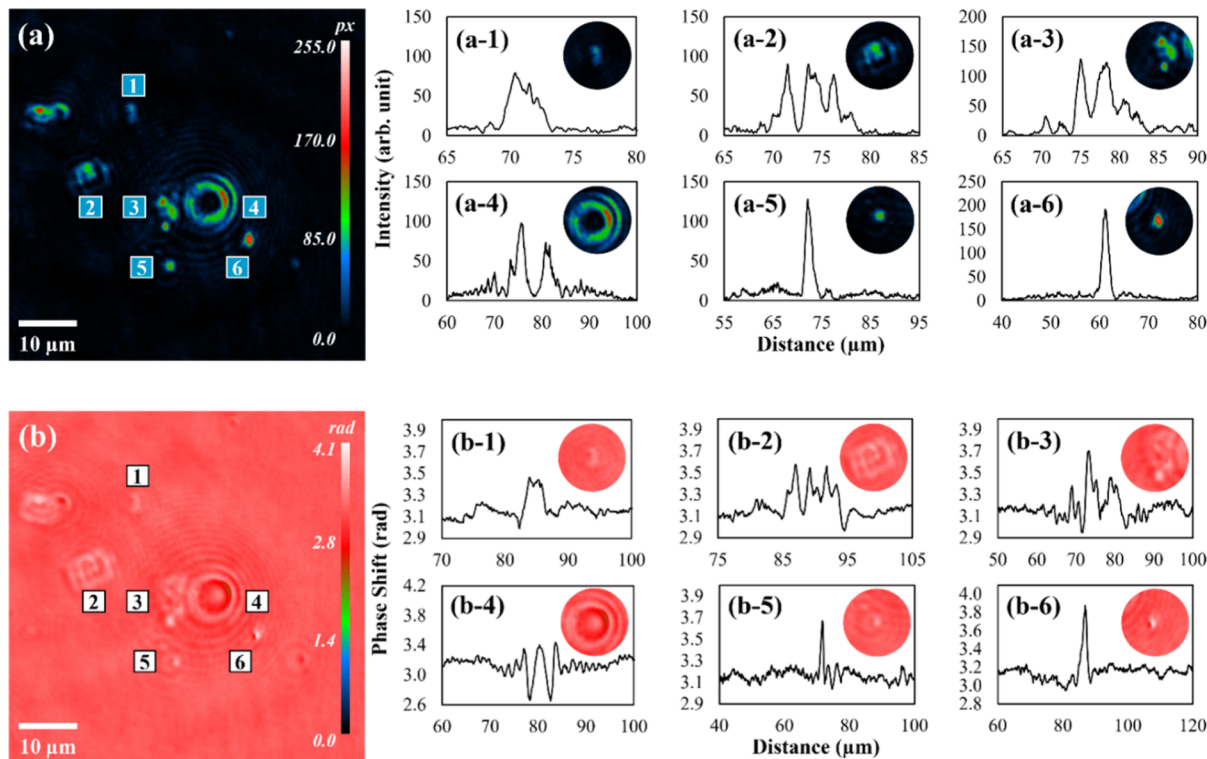


Figure 2. Reconstructions of nanoplastics and nonplastic particles within a mixture. (a) Intensity images and crosscuts of (a-1) magnetite, (a-2, a-3) phytoplankton, (a-4) oleic acid, (a-5) likely PS nanoplastic particle, and (a-6) likely PE. (b) Phase reconstructions with respect to panel (a), $z = 332 \mu\text{m}$.

3. RESULTS AND DISCUSSION

3.1. Detection of Nano- and Microplastics: Intensity and Phase. Figure 1 demonstrates that nano-DIHIM can detect polyethylene (PE) nano/microplastic particles within a broad size range, from 197 nm to over 4 mm in water. The upper size boundary reaches 6 mm, and the lower size limit can go below 100 nm by improved numerical reconstruction approaches and optimized experimental setups.^{31,33,43} The smallest plastic particles detected in this work are 50 nm polystyrene latex beads (PSL). Yet, it is important to note that most of the beads are seen as dimers or trimers; due to the current lateral resolution limit, they are identified as a single particle (Figure S7a).³¹

The intensity and phase reconstructions (images and crosscuts) of different particles exhibit unique and distinct characteristics, unveiling particle sizes, shapes, homogeneities/heterogeneities, and coatings (Figures 1 and S7). For instance, the reconstruction images show a single point, and the crosscuts exhibit a unimodal peak when a PE nanoplastic particle is solely presented (Figure 1a,e). The images of an oleic acid droplet show a bright round-shaped center encircled by expanding ripples arising from the interferences of the light, where the crosscuts exhibit symmetric multimodal peaks with the highest signal in the middle and attenuating signals away from the apex (Figure S7b-13,c-13). When an oleic acid coated PE is examined, the images present layers of halos resulting from the organic coating with a distorted pattern due to the presence of the PE core (Figure 1b,f). Reflected in the crosscuts is a signal distribution overall that resembles that of a single oleic acid droplet but with an asymmetric pattern.

In addition to PE, nano-DIHIM can detect many types of nano/microplastics, organics, inorganics, and biological

materials. They include polypropylene (PP), polystyrene (PS), polyethylene terephthalate (PET), polyurethane (PUR), polyvinyl chloride (PVC), magnetite, titanium dioxide, oleic acid, humic acid, and phytoplankton. Each type of material produces distinctive intensity and phase features for particle identification (Note S11 and Figure S7). Different core materials can also be detected when they are covered by organic layers, reflected by the distinct intensity and phase reconstruction images and crosscuts (Figures 1b,f and S7d-1–d-4). TEM images confirm the particle size and shape data of model nanoplastic particles obtained using nano-DIHIM (Figure S7e-1–e-4).

3.2. Distinguishing Nano/Microplastics from Non-plastic Particles. Plastic particles rarely stay isolated in the environment, they form heteroaggregates with other natural and anthropogenic substances.⁴⁴ Nano-DIHIM can identify single and multiple particles concurrently. Figure 2 demonstrates that nano-DIHIM distinguishes nano/microplastics and nonplastics from a heterogeneous blend of PE, PS, oleic acid, magnetite, and phytoplankton in water. By comparing the shapes and crosscuts of the mixed particles (Figure 2) and reference particles (Figures 1 and S7), particle 1 is determined to be magnetite; particles 2 and 3 display specific features of phytoplankton, and particle 4 is an oleic acid droplet.

Although the reconstruction results of certain materials exhibit distinct characteristics and reveal the identity of the substances, nanoplastic particles sharing similar physicochemical properties can have highly similar reconstruction images and particle crosscuts, posing a challenge for identification. Particles 5 and 6 in Figure 2 are likely PS and PE nanoplastics, respectively, based on the particle shape and size information. An accurate classification of these two types of nanoplastics is

Table 1. Autocharacterization and Classification of Nanoplastics and Nonplastics in a Water Sample by a Deep Neural Network Image Classifier in the Laboratory^a

Shape	Length (μm)	Width (μm)	Perimeter (μm)	Surface area (μm ²)	Surface roughness	Edge gradient	Taxon
	*(0.33)	*(0.33)	3.73	0.94	1.05	120.19	PE
	*(0.38)	*(0.36)	4.32	1.32	1.06	116.87	PE
	*(0.39)	*(0.35)	4.00	0.99	1.02	62.97	PS
	*(0.48)	*(0.48)	5.54	2.07	1.02	50.49	PS
	*(4.14)	*(2.53)	62.46	58.12	1.76	81.80	Magnetite
	*(1.05)	*(0.72)	10.85	6.60	1.13	104.83	Magnetite
	*(4.22)	*(4.22)	47.78	176.30	1.04	58.16	Oleic Acid
	*(5.33)	*(4.79)	70.02	257.02	1.27	73.96	Oleic Acid
	*(2.28)	*(1.62)	30.54	28.69	1.44	64.32	Phytoplankton
	*(1.62)	*(1.46)	25.93	22.65	1.43	58.15	Phytoplankton
	*(0.45)	*(0.45)	5.01	1.50	1.01	61.19	Not Identified
	*(0.40)	*(0.40)	4.61	1.32	1.01	89.89	Not Identified

^aThe autoreconstructed images with morphological parameter data extracted by 4Deep Stingray software are tabulated. The corrected particle length and width data (based on eq 5 in Methods^{39,40}) are provided in *().

achieved by incorporating additional parameters (e.g., surface area, roughness, and edge gradient) into a deep neural network, as presented in Section 3.3.

The particles lay on separate z-directional planes within the studied volume. Reconstructions on several z-planes are thus required to bring the objects into focus (Note S4 and Video S1). The object is in shades of cyan when it is partially out of focus (Figure 2a-1). Notably, the presence of a cyan layer around a red core (Figure 2a-5,a-6) indicates the development of polymer layers and hydration shells over the nanoplastics in water, leading to an overestimated particle size.^{45,46} Such an overestimation is also reflected in the widened peak baselines on the crosscuts.

3.3. Automated Particle Characterization and Classification. The identification processes are laborious for many techniques when the number of samples increases. The background signals could further complicate the data acquisition, especially when the particles share similar, but not identical, morphologies and chemical compositions.⁴⁷ Incorporating artificial intelligence allows fast and accurate particle detection.^{47–49} We herein deploy automated characterization and classification of nano/microplastics and nonplastic particles using a deep neural network in combination with nano-DIHM.^{32,38} See Note S5 for additional information on the automation workflow and the classifier training processes.

Table 1 presents the autoclassification output of the same mixture sample seen in Figure 2, using a classifier trained with PE, PS, magnetite, oleic acid, and phytoplankton taxa. The particle physicochemical properties, including shape, size, perimeter, area, surface roughness, and edge gradient, are automatically extracted and compared (Table 1).

Over 85% of the autocharacterized PE nanoplastics bear similar roughness ranging from 1.03 to 1.09 and edge gradient values from 96.25 to 122.47. This similarity can be attributed to the fact that these particles are synthesized by using the same material and method. Likewise, the roughness (1.00–1.04) and edge gradient (49.01–83.90) values for all PS nanoplastics are comparable. Such parameters of PE and PS are discriminative for the deep neural network to distinguish the two types of widely used plastics. As of other materials, for instance, magnetite, the roughness has a broader range from 1.09 to 1.82, and the edge gradient is from 78.02 to 107.14. This observation can be explained by the formation of magnetite clusters in different sizes and structures, which agrees with the manual reconstruction observations (Figures S7). Such results also suggest the potential of AI-assisted nano-DIHM in investigating the physical processes and transformation mechanisms of diverse particles/clusters in the environment.³⁵

Nevertheless, it should be noted that the automation yields only particle size $>1\ \mu\text{m}$ mainly due to the tendency of the algorithm to overestimate the particle size. For instance, the size of studied PE and PS nanoplastics is between 100 and 800 nm, but the software measures $\sim 1.1\text{--}1.8\ \mu\text{m}$ for most plastic particles. Such deviations in size measurements have been frequently observed in DIHM research, especially when automated processing is involved.^{40,50,51} Although the reasons behind it have not been fully understood, factors such as source-to-object distances, the algorithm programming, and the actual particle size could affect the degree of the deviation.^{39,40,50–52} For example, it is observed that the size of the smaller particles can be more severely overestimated compared to the larger ones.⁵² Thus, various size correction approaches are employed to retrieve the accurate particle size information.^{39,40,51,52} Table 1 provides particle length and width values after size correction based on previous research.^{39,40} Further development and incorporation of improved machine vision algorithms may advance accurate nanoplastic detection.^{53,54}

Extrapolating laboratory findings to real-world applications presents challenges. Nanoplastics are highly likely to associate or attach to abundant anthropogenic particles and natural products, which alters their presence and complicates the detection.^{44,55} The lack of efficient approaches for identification/quantification further hinders the comprehensive understanding of the abundance and distribution of environmental nanoplastics.^{56,57} In the following section, we provide additional evidence for the capability of AI-assisted nano-DIHM as a portable sensor and high-throughput tool for the rapid detection of nano- and microplastics in environmental waters.

3.4. Automated Detection of Nano/Microplastics in Natural Waters. Physicochemical features of over 20,000 nano- and microsized ($<1000\ \mu\text{m}$) waterborne particles are automatically extracted from $3 \times 4\ \text{mL}$ of environmental waters obtained from Lake Ontario. The particles are subsequently autoclassified using a validated classifier ($>95\%$ confidence) trained with a “Nanoplastics” taxon and a “Lake Ontario” taxon (Note S7).

On average 2% of the total particles in Lake Ontario water samples are identified as nano/microplastics, 94% are nonplastics, and 4% are unclassified (Figure 3a). Among the 453 particles detected in the same amount of the field blanks, 1 particle is classified as nano/microplastics (Note S12 and Figure S8). The autoclassification is performed systematically for Saint Lawrence River waters using AI-assisted nano-DIHM, where 1% of the river-borne particles are identified as nano/microplastics, 98% are nonplastic particles, and 1% are not identified (Note S12 and Figure S9). The result of a positive control (i.e., spiked experiment) shows a significant increase in the number of particles (33%) identified as nano/microplastics (Note S12 and Figure S10).

Multiple efforts are made to determine the research strategies best suited for autodetecting nano/microplastics in environmental waters. The three major considerations are discussed in the following.

First, we strive to inspect all particles possible throughout the water volume by analyzing 1000 reconstruction planes for each hologram, with a z-directional searching distance from 1 to $8000\ \mu\text{m}$. Yet, some particles could still be overlooked. Increasing the number of reconstruction planes and conducting multiple runs with segmented searching distances (e.g., 1–

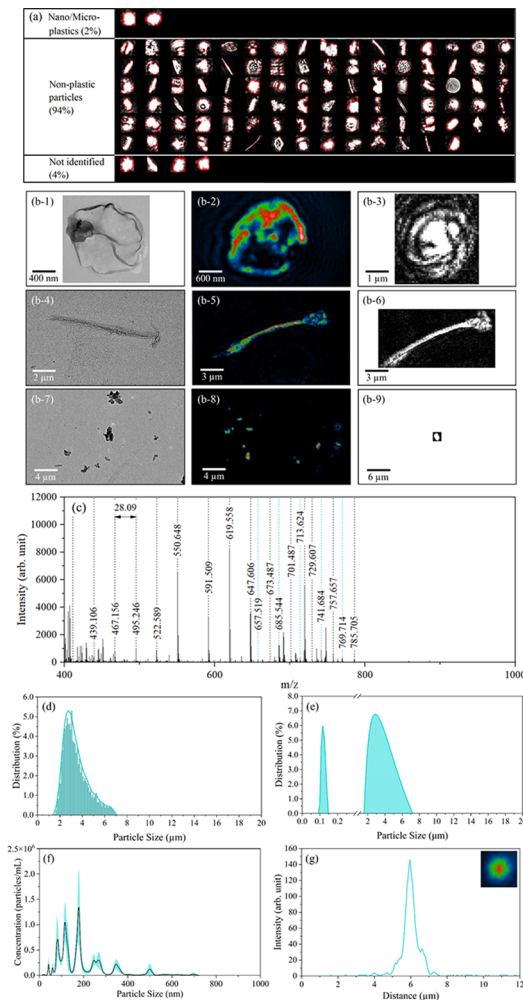


Figure 3. Rapid autoclassification of nano/microplastics and nonplastics in environmental waters (Lake Ontario) in dynamic using AI-assisted nano-DIHM; data validation by high-resolution transmission electron microscopy (HR-TEM), nanostructured laser desorption/ionization time-of-flight mass spectrometry (NALDI-TOF-MS), and particle size analysis. (a) Automated classification of over 20,000 particles in Lake Ontario water. Presented are 100 examples acquired by Stingray software. (b) Comparison of waterborne particle images by (b-1, b-4, b-7) TEM, (b-2, b-5, b-8) nano-DIHM manual reconstructions by Octopus software, and (b-3, b-6, b-9) automated reconstructions by Stingray software. (c) Confirmation of the presence of polyethylene by NALDI-TOF-MS. Also, particle size distribution of the waterborne particles based on (d) corrected particle size extracted by automation and (e) dynamic light scattering by aquatic particle size analysis. (f) The concentration of the waterborne particles on the nanoscale is measured using nanoparticle tracking analysis. (g) The intensity crosscut of a nanosize particle in the Lake Ontario sample acquired by nano-DIHM manual reconstruction.

4000 μm followed by 4000–8000 μm rather than covering 1–8000 μm at once) can improve the particle finding performance, but these can cause prolonged processing time. In this study, the particle characterization rate is ~ 1.4 objects per second and the classification rate is 25 objects per second. Such processes can be shortened by increasing the intensity threshold for image extraction and database scrubbing.

Second, at the beginning of this work, we expect AI-assisted nano-DIHM to identify different types of plastics. A classifier trained using six taxa of different types of nano/microplastics,

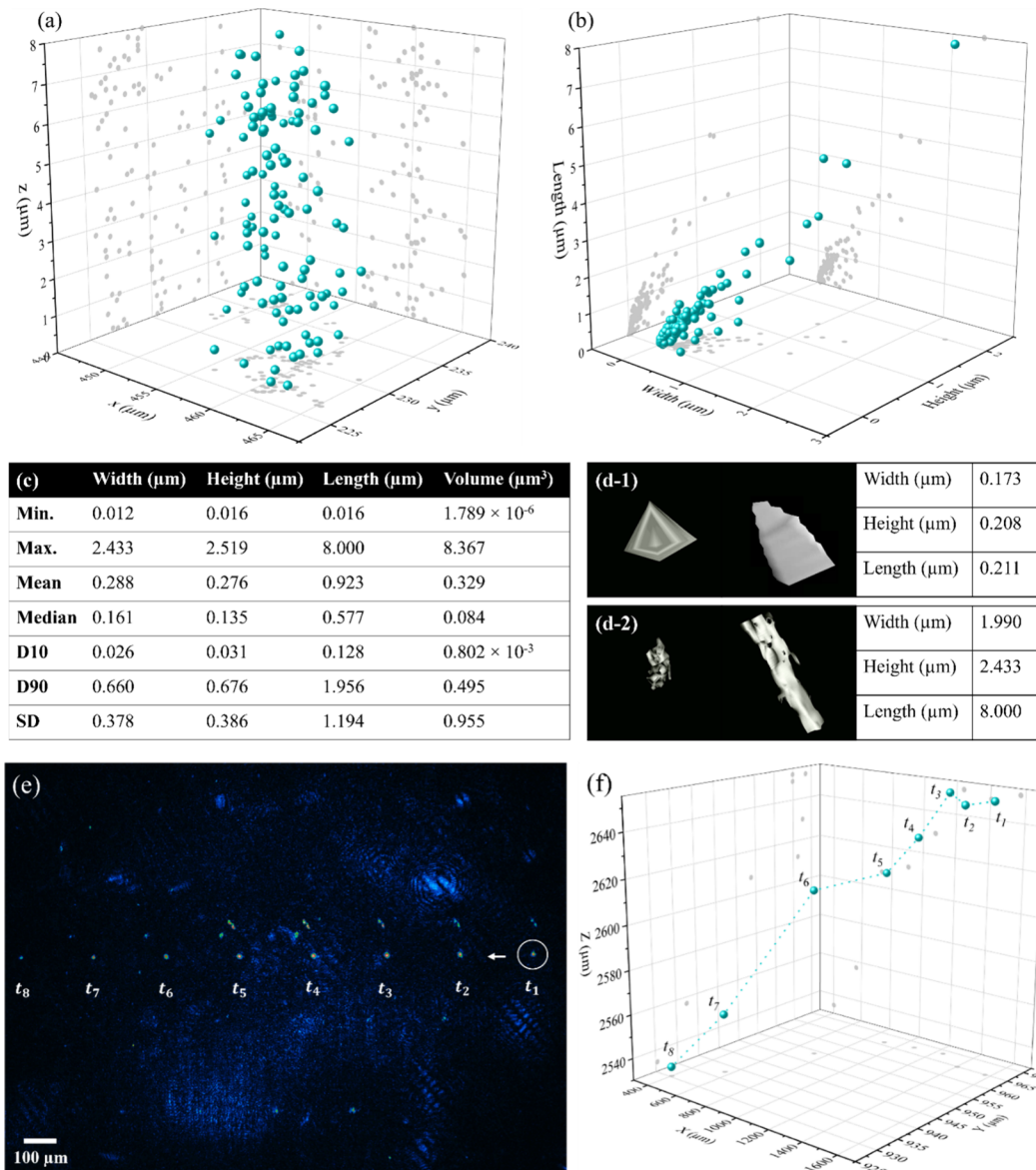


Figure 4. 3D particle size and spatial distribution analysis and 4D real-time in situ dynamic tracking of waterborne particles. (a) The spatial distribution of 113 waterborne particles in a single hologram. (b) The 3D particle dimensions of the 113 particles in respect of panel (a). (c) A table of particle size and volume statistics regarding the 113 waterborne particles. (d-1, d-2) Two examples of the 3D display and particle size data obtained by 3D reconstruction. (e) A compilation of eight consecutive intensity reconstruction images of waterborne particles in dynamic. (f) The 4D (3D + time) trajectory of the same particle circled in panel (e). The 3D and 4D reconstructions are obtained by Octopus software.

including PE, PP, PS, PET, PUR, and PVC, fails the validation test with <15% confidence. This failure can be explained by the similar roughness and edge gradient values of some plastics compared to others (Note S7 and Table S2). Since AI-assisted nano-DIHM cannot distinguish many different types of nano/microplastics at the current stage, the autocharacterization data of PE, PP, PS, PET, PUR, and PVC are unified under one taxon named “Nanoplastics” instead of being allocated to individual taxa of the corresponding plastics. A classifier is trained using the “Nanoplastics” taxon and the “Lake Ontario” (or “Saint Lawrence River”) taxon, which is subsequently applied to autoclassify the environmental samples.

Lastly, plastic fragments possess irregular shapes, such as film, fiber, foam, and granules.⁵⁸ The surface morphologies of aged nano/microplastics are likely rougher than the pristine ones, introducing uncertainties in the autoclassification.

The “Nanoplastics” taxon is fed with data of the more controllable plastics prepared in the laboratory rather than the intricate real environmental nano/microplastics because isolating real-world environmental nano/microplastics is already an identified challenge. This work is still at its pioneering stage to prove that AI-assisted nano-DIHM is a novel capability for autocharacterization and classification of nano/microplastics in environmental samples. Our future work will prioritize integrating physicochemical data of aged nano/microplastics with different sizes and shapes into the database of the deep neural network.

3.5. Validation of Nano-DIHM Results and Complementary Analysis. Figure 3b demonstrates that the morphologies of the waterborne particles acquired using transmission electron microscopy (TEM) can be concurrently observed using AI-assisted nano-DIHM. For instance,

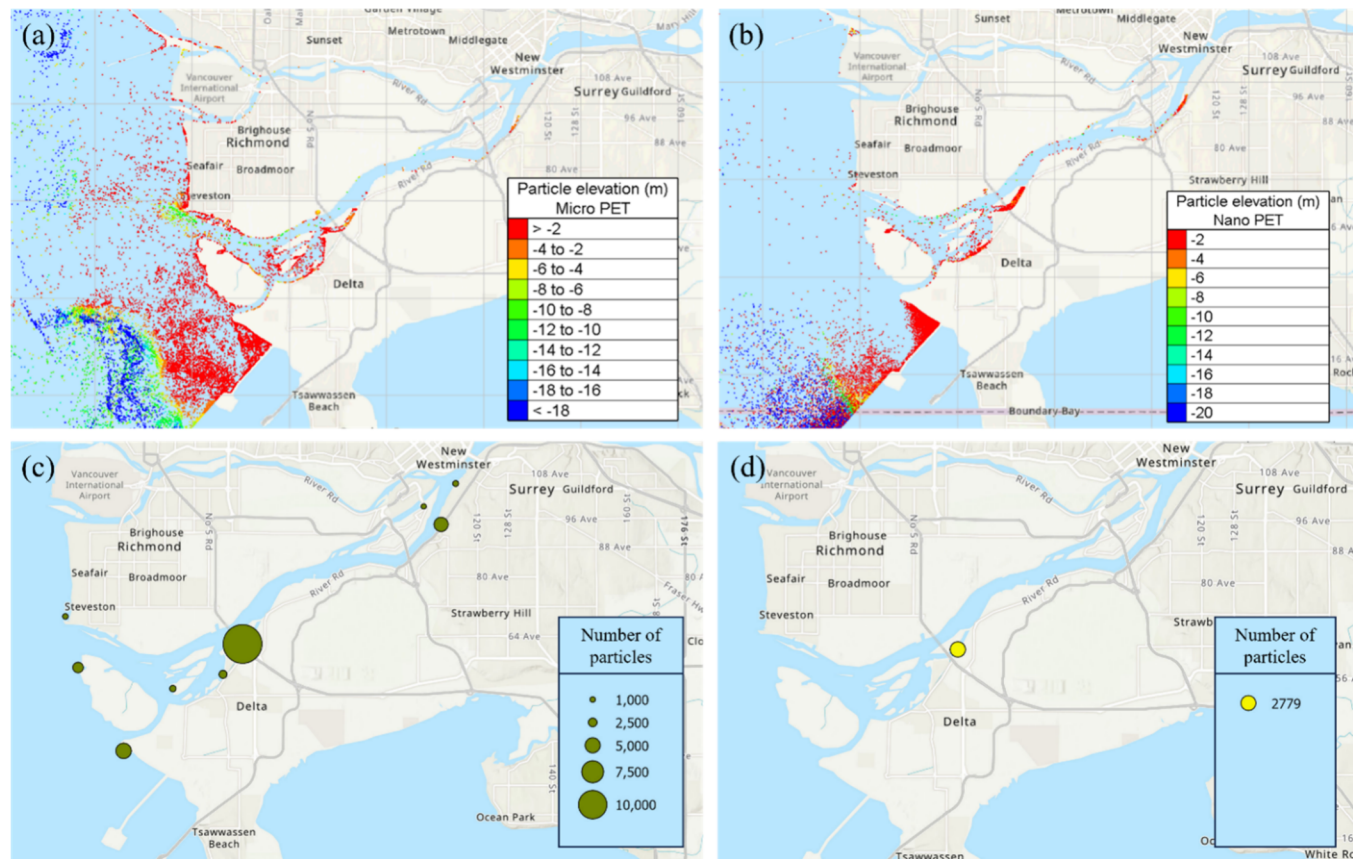


Figure 5. Model results of the distributions and predicted accumulation zones of studied micro- and nanosized plastic particles. Modeled distribution of (a) microsized polyethylene terephthalate (PET) and (b) nanosized PET plastic particles in the modeling domain on day 16 of the simulation. The predicted accumulation zones of the studied (c) micro-PET and (d) nano-PET particles between Douglas Island and the Strait of Georgia.

layered and fibrous structure seen by TEM is of a similar shape and size to the particles presented in the manual reconstructions and the autoextracted images acquired utilizing nano-DIHM. Yet, it is not suggested that these particles are representing the same particles. Figure 3b–7–b–9 demonstrates that nano-DIHM can detect single and multiple/aggregate particles simultaneously.

Nanostructured laser desorption/ionization time-of-flight mass spectrometry (NALDI-TOF-MS) analysis of the water samples displays a series of signals with $\sim 28\text{ m/z}$ intervals, indicating the presence of polyethylene (PE) in Lake Ontario waters (Figure 3c). This observation is consistent with the detection of nano/microplastics in the water samples by the autocharacterization and classification of AI-assisted nano-DIHM.

Figure 3d depicts the 2D particle size distribution of the Lake Ontario samples based on the autoextracted data after size correction, showing a skewed monomodal curve peaked at $\sim 3\text{ }\mu\text{m}$. A bimodal distribution with signal maximums at $3.3\text{ }\mu\text{m}$ and 120 nm is observed for the same samples, using an aquatic particle size analyzer (Figure 3e). The particle size analyzer data confirmed the results acquired using automated nano-DIHM in the micro/submicron range. Yet, the automation functionality still requires further efforts, such as image denoising processes, to allow for improved particle size analysis in the nanoscale.^{61,62} Nanoparticle tracking analysis implies the abundance of waterborne particles on the nanoscale, especially under 200 nm , confirming the observa-

tions of nano- and submicrometer-sized waterborne particles by manual reconstruction using nano-DIHM (Figure 3f,g).

The same experiments are conducted systematically for the Saint Lawrence River waters. Particle images acquired using nano-DIHM are consistent with the images obtained by TEM. NALDI-MS confirms the presence of nano/microplastics, specifically polytetrahydrofuran (PTHF), in the river waters. See Note S12 for complete results. Additional metal and total organic carbon (TOC) data exhibit the complexity of the environmental waters and confirm the observations of diverse particles and clusters from nano-DIHM (Table S3).

Digital in-line holographic microscopy (DIHM) can detect various materials, such as biological cells, oil droplets, heavy metals and metal oxides, mineral dusts, and snowflakes, in water and air.^{32,63–65} AI-assisted nano-DIHM has a broad scope of applications for detecting nano/microplastic particles and promptly characterizing a wide range of emerging contaminants and hazardous substances in different environmental and biological matrices.

3.6. 3D Physicochemical and Spatial Data and 4D Dynamic Tracking. Nano-DIHM allows for 3D particle size, shape, volume, and spatial distribution analysis. Figure 4 depicts the 3D positions (XYZ orientations) of 113 waterborne particles captured within the studied volume in a single hologram. The particle dimensions (width, height, length, and volume) of the 113 particles are plotted in Figure 4b and tabulated in Figure 4c. The 10th percentiles of the particle dimensions are 26 nm (width), 31 nm (height), and 128 nm

(length), confirming the capability of nano-DIHM in detecting nanoparticles. The particle length values are overestimated, because when the distance between two particles is smaller than the depth resolution, the algorithm treats two particles as one.³¹ The 3D images and size information on every individual particle are available for volumetric geometric studies. Presented in Figure 4d-1,d-2 are two representative lakeborne particles.

Nano-DIHM can track real-time and in situ 4D (3D + time) dynamics of nano/microplastic particles and nonplastic particles in water. Figure 4e is a compilation of a series of consecutive intensity reconstructions of waterborne particles in dynamic mode, where the particles pass through the instrument horizontally with the water flow. Video S2 shows a dynamic recording. Corresponding 4D data indicate that although the particle moves horizontally with the fluid, it moves downwardly in the z-direction due to gravity (Figure 4f). Such dynamic processes are crucial for model studies to predict the transportation and accumulation of nano/microplastics in aquatic systems, providing the means to evaluate hazard exposures and implement remediation strategies.^{26,28} A control experiment is performed using 200 nm PSL, as demonstrated in Note S13, Figure S11, and Video S3.

3.7. Distinct Distributions of Nano- and Microplastics by Model. In this section, we highlight the significance of precise data input on the characteristics and dynamics of nano/microplastics for informing fate and transport modeling in aquatic systems. We conduct a modeling study of nanosized (800 nm) and microsized (50 μm) PET plastic particles in the Fraser River, in British Columbia, Canada, to showcase the practical implications of nano-DIHM.

The CaMPSim-3D model is used to explore the distribution patterns of nano/microplastic particles in natural waters. The transport in CaMPSim-3D is simulated by solving the advection–diffusion in eq 7) for all the modeled microsized plastics, where Dx_p is the particle displacement in time step Dt , U_p denotes the particle velocity, R is a random number between -1 and 1, and K is the dispersion coefficient representing the calculated turbulence characteristics of the ambient flow.^{25,28}

$$\frac{Dx_p}{Dt} = U_p + \frac{DU_p}{Dt} U_p Dt + \frac{R\sqrt{2K}Dt}{Dt} \quad (7)$$

where

$$\frac{DU_p}{Dt} = \frac{1}{2} \left(U \cdot \nabla U + \frac{\partial U_p}{\partial t} \right) \quad (8)$$

As CaMPSim-3D is initially developed for microplastics, the advection–diffusion equation is modified by adding a new term to the right-hand side of eq 7 to represent Brownian motion. This modification enables the modeling displacement of nanoplastics as the result of Brownian diffusion (Dif_b), as shown in eq 9:

$$Dif_b = \frac{\int_0^{Dt} R \sqrt{2K_b} Dt_b}{Dt} \quad (9)$$

where $Dt_b = 0.9$ s is the time step of Brownian motion, and $K_b = 1 \text{ m}^2/\text{s}$ is the Brownian diffusion coefficient.

Figure 5 demonstrates the simulated distribution patterns of nano- and microplastic particles within the modeling domain 17 days after their release. A notably difference is observed

across the water surface and through the water column. The particle distributions at the end of the simulations are used as inputs in a machine learning-based clustering model to identify the accumulation zones.⁴¹ Results suggest that 33.2% of the microplastics stay within the river domain, compared to 3.7% of the nanoplastics (Figure 5c,d). This finding suggests that microplastics have a higher propensity to remain within the Fraser River, while nanoplastics tend to travel greater distances from the point of release, with a significant number of particles reaching the ocean. These observations emphasize the distinct behaviors and distribution patterns (i.e., dispersion and elevation) of nano- and microplastics in aquatic systems. The animations depicting the dynamics of nano- and microplastic transport processes are in Videos 4 and 5.

3.8. Implications of the Real-Time and In Situ Technology. In situ sensors are widely used for water quality applications, particularly in remote regions, where the costs and logistics of sampling and laboratory testing can be prohibitive.^{66–68} The advantages offered by in situ and real-time monitoring systems, including timely data retrieval, and expanded spatial and temporal coverage, can be leveraged to enhance field measurements and data collection, improve accuracy of predictive modeling, and facilitate effective decision making.^{69–71} Hence, in situ and real-time technologies capable of determining the distribution and physicochemical characteristics of nano/microplastics, thus the impacts or mitigations of nano/microplastic pollution on human health and aquatic ecosystems, are needed for effective regulation and management purposes.^{71–74}

Despite commercially available water quality sensors, which offer capabilities to detect a select set of physicochemical and biological parameters, like conductivity/salinity, dissolved oxygen, pH, turbidity, chlorophyll, and temperature, to the best of our knowledge, there is not any proven in situ and real-time sensor technology to detect and characterize nanoplastic particles in water.^{74–76} Recent advances in employing underwater spectral imaging and evolving image processing have improved the quality of underwater object detection in different turbid waters.^{77–80} This laboratory has also demonstrated that detecting materials in turbid water is still feasible using nano-DIHM with a minimum light penetration.³² In situ flow-through sensors that can provide real-time physicochemical data on the quantity and characteristics of nano/microplastics in water, like the AI-assisted nano-DIHM developed in this work, can be used to develop scalable monitoring systems for different aquatic ecosystems.

3.9. Future Directions. The development and application of AI-assisted nano-DIHM represent a significant milestone in tackling environmental and health issues caused by (nano/micro)plastics. In this research, AI-assisted nano-DIHM provides quantified physicochemical parameters of nano/microplastics, 3D particle size and spatial information, and 4D dynamic tracking. Future improvements in number density quantification and in-depth surface characteristics will expand the application of AI-assisted nano-DIHM. This work serves a broad range of research and technologies, from time-dependent physical and chemical transformations of various contaminants, biogeochemistry, and life-cycle analysis of environmental pollutants in the Earth's aquatic system to sustainable remediation and management of marine plastic pollution.

ASSOCIATED CONTENT

Data Availability Statement

All relevant data that support the findings of this study are presented in the main text and *Supporting Information*. The full data will be available upon request.

SI Supporting Information

The Supporting Information is available free of charge at <https://pubs.acs.org/doi/10.1021/acs.est.3c10408>.

Comparison of techniques for the detection of environmental nanoplastics (Note S1 and Table S1); the principle of digital in-line holographic microscopy (DIHM) (Note S2 and Figure S1); preparation of nanoplastics and suspensions of analytes (Note S3); reconstruction planes of the 3D volume (Note S4 and Figure S2); automated particle characterization and classification (Note S5 and Figure S3); the assessment of river-borne nano/microplastics in dynamic mode (Note S6 and Figures S4 and S5); the nanoplastic taxon for the autoclassification of environmental samples (Note S7 and Table S2); validating AI-assisted nano-DIHM data using complementary techniques (Note S8); instruments, materials, and supplies (Note S9); modeling study of the transport and fate of nano- and microplastics (Note S10 and Figure S6); nano-DIHM for detecting various nano- and microplastics and nonplastic particles (Note S11 and Figure S7); physicochemical analysis of Saint Lawrence River samples and blanks/controls (Note S12, Figures S8–S10, and Table S3); the control of the 3D and 4D data (Note S13 and Figure S11) ([PDF](#))

Intensity reconstructions of a single hologram at different z-planes ([MP4](#))

Conservative intensity reconstructions of a flowing natural water sample ([MP4](#))

Conservative intensity reconstructions of the movement of 200 nm PSL beads injected into water ([MP4](#))

Particle elevation (m) of micro-PET ([MP4](#))

Particle elevation (m) of nano-PET ([MP4](#))

AUTHOR INFORMATION

Corresponding Author

Parisa A. Ariya – Department of Chemistry, McGill University, Montreal, Quebec H3A 0B8, Canada; Department of Atmospheric and Oceanic Sciences, McGill University, Montreal, Quebec H3A 0B9, Canada;  orcid.org/0000-0001-5269-5017; Email: parisa.ariya@mcgill.ca

Authors

Zi Wang – Department of Chemistry, McGill University, Montreal, Quebec H3A 0B8, Canada;  orcid.org/0000-0001-9966-2968

Devendra Pal – Department of Atmospheric and Oceanic Sciences, McGill University, Montreal, Quebec H3A 0B9, Canada

Abolghasem Pilechi – National Research Council Canada, Ottawa, Ontario K1A 0R6, Canada

Complete contact information is available at:
<https://pubs.acs.org/doi/10.1021/acs.est.3c10408>

Author Contributions

Z.W. performed most work of this research and drafted the current paper. D.P. helped with the experiments and revised

the manuscript. A.P. performed the model study and wrote the modeling sections of this paper. P.A.A. wrote the funded proposal, which provides the basis of this work, supervised Z.W. and D.P., and revised the manuscript.

Notes

The authors declare no competing financial interest.

All authors have been trained in Equity, Diversity, and Inclusion (EDI) principles at McGill University and the National Research Council of Canada. They have all participated in ethical workshops to ensure an environment of equity, diversity, and inclusion throughout this project. The authors are from diverse backgrounds.

ACKNOWLEDGMENTS

This work was supported by Canadian Foundation for Innovation (CFI) [259754], Natural Science and Engineering Research Council of Canada (NSERC) [223464], National Research Council Canada (NRC) [257365], and Prima Quebec [257058]. We would like to thank Ryan Hall for proofreading of the manuscript. We acknowledge Zhe Li for helping with sampling. We acknowledge Nadim K. Saadé and David Liu at McGill University for performing MALDI-TOF-MS and HR-TEM analysis. We would like to thank Maria Chrifi Alaoui, Belanger Dominic, and Marc Amyot at University of Montreal for providing QQQ-ICP-MS/MS results, Katherine Velghe at University of Quebec in Montreal for performing TOC analysis, and Laura Montermini and Janusz Rak at Montreal Children's Hospital - McGill University Health Centre for providing NTA data.

REFERENCES

- (1) Yee, M. S.; Hii, L. W.; Looi, C. K.; Lim, W. M.; Wong, S. F.; Kok, Y. Y.; Tan, B. K.; Wong, C. Y.; Leong, C. O. Impact of microplastics and nanoplastics on human health. *Nanomaterials* **2021**, *11* (2), 496.
- (2) Cunningham, B. E.; Sharpe, E. E.; Brander, S. M.; Landis, W. G.; Harper, S. L. Critical gaps in nanoplastics research and their connection to risk assessment. *Front. Toxicol.* **2023**, *5*, No. 1154538.
- (3) Materic, D.; Kjaer, H. A.; Vallelonga, P.; Tison, J. L.; Rockmann, T.; Holzinger, R. Nanoplastics measurements in Northern and Southern polar ice. *Environmental Research* **2022**, *208*, No. 112741.
- (4) Xie, L.; Gong, K.; Liu, Y.; Zhang, L. Strategies and challenges of identifying nanoplastics in environment by surface-enhanced Raman spectroscopy. *Environ. Sci. Technol.* **2023**, *57* (1), 25–43.
- (5) Wang, Z.; Saadé, N. K.; Ariya, P. A. Advances in ultra-trace analytical capability for micro/nanoplastics and water-soluble polymers in the environment: Fresh falling urban snow. *Environ. Pollut.* **2021**, *276*, No. 116698.
- (6) Morales, A. C.; Tomlin, J. M.; West, C. P.; Rivera-Adorno, F. A.; Peterson, B. N.; Sharpe, S. A. L.; Noh, Y.; Sendesi, S. M. T.; Boor, B. E.; Howarter, J. A.; Moffet, R. C.; China, S.; O'Callahan, B. T.; El-Khoury, P. Z.; Whelton, A. J.; Laskin, A. Atmospheric emission of nanoplastics from sewer pipe repairs. *Nat. Nanotechnol.* **2022**, *17* (11), 1171–1177.
- (7) Ter Halle, A.; Jeanneau, L.; Martignac, M.; Jarde, E.; Pedrono, B.; Brach, L.; Gigault, J. Nanoplastic in the North Atlantic subtropical gyre. *Environ. Sci. Technol.* **2017**, *51* (23), 13689–13697.
- (8) Kakar, F. L.; Okoye, F.; Onyedibe, V.; Hamza, R.; Dhar, B. R.; Elbeshbishi, E., Climate change interaction with microplastics and nanoplastics pollution. *Current Developments in Biotechnology and Bioengineering*; Elsevier, 2023. Chapter 16, 387–403.
- (9) Ganguly, M.; Ariya, P. A. Ice nucleation of model nanoplastics and microplastics: A novel synthetic protocol and the influence of particle capping at diverse atmospheric environments. *ACS Earth and Space Chemistry* **2019**, *3* (9), 1729–1739.

- (10) Aeschlimann, M.; Li, G.; Kanji, Z. A.; Mitrano, D. M. Potential impacts of atmospheric microplastics and nanoplastics on cloud formation processes. *Nature Geoscience* **2022**, *15* (12), 967–975.
- (11) Liu, X.; Wang, S.; Mu, L.; Xie, Y.; Hu, X. Microplastics reshape the fate of aqueous carbon by inducing dynamic changes in biodiversity and chemodiversity. *Environ. Sci. Technol.* **2023**, *57* (28), 10415–10425.
- (12) Mitrano, D. M.; Wick, P.; Nowack, B. Placing nanoplastics in the context of global plastic pollution. *Nat. Nanotechnol.* **2021**, *16* (5), 491–500.
- (13) Gigault, J.; Halle, A. T.; Baudrimont, M.; Pascal, P. Y.; Gauffre, F.; Phi, T. L.; El Hadri, H.; Grassl, B.; Reynaud, S. Current opinion: What is a nanoplastic? *Environ. Pollut.* **2018**, *235*, 1030–1034.
- (14) Mandemaker, L. D. B.; Meirer, F. Spectro-microscopic techniques for studying nanoplastics in the environment and in organisms. *Angew. Chem., Int. Ed.* **2023**, *62* (2), No. e202210494.
- (15) Yang, Q.; Zhang, S.; Su, J.; Li, S.; Lv, X.; Chen, J.; Lai, Y.; Zhan, J. Identification of trace polystyrene nanoplastics down to 50 nm by the hyphenated method of filtration and surface-enhanced Raman spectroscopy based on silver nanowire membranes. *Environ. Sci. Technol.* **2022**, *56* (15), 10818–10828.
- (16) Foetisch, A.; Filella, M.; Watts, B.; Vinot, L. H.; Bigalke, M. Identification and characterisation of individual nanoplastics by scanning transmission X-ray microscopy (STXM). *Journal of Hazardous Materials* **2022**, *426*, No. 127804.
- (17) Cai, H.; Xu, E. G.; Du, F.; Li, R.; Liu, J.; Shi, H. Analysis of environmental nanoplastics: Progress and challenges. *Chemical Engineering Journal* **2021**, *410*, No. 128208.
- (18) Roberto de Bruin, C.; de Rijke, E.; van Wezel, A. P.; Astefanei, A. Methodologies to characterize, identify and quantify nano- and sub-micron sized plastics in relevant media for human exposure: a critical review. *Environmental Science: Advances* **2022**, *1* (3), 238–258.
- (19) Alice, P.; Maud, G.; Dominique, B.; Julien, G. Micro- and nanoplastic transfer in freezing saltwater: implications for their fate in polar waters. *Environmental Science: Processes & Impacts* **2021**, *23* (11), 1759–1770.
- (20) Chen, C.; Sun, C.; Wang, B.; Zhang, Z.; Yu, G. Adsorption behavior of triclosan on polystyrene nanoplastics: The roles of particle size, surface functionalization, and environmental factors. *Sci. Total Environ.* **2024**, *906*, No. 167430.
- (21) Caputo, F.; Vogel, R.; Savage, J.; Vella, G.; Law, A.; Della Camera, G.; Hannon, G.; Peacock, B.; Mehn, D.; Ponti, J.; Geiss, O.; Aubert, D.; Prina-Mello, A.; Calzolai, L. Measuring particle size distribution and mass concentration of nanoplastics and microplastics: addressing some analytical challenges in the sub-micron size range. *J. Colloid Interface Sci.* **2021**, *588*, 401–417.
- (22) Sharma, V. K.; Ma, X.; Lichtfouse, E.; Robert, D. Nanoplastics are potentially more dangerous than microplastics. *Environmental Chemistry Letters* **2023**, *21* (4), 1933–1936.
- (23) Bhat, M. A.; Gedik, K.; Gaga, E. O. Atmospheric micro (nano)plastics: future growing concerns for human health. *Air Quality, Atmosphere & Health* **2023**, *16* (2), 233–262.
- (24) Gigault, J.; El Hadri, H.; Nguyen, B.; Grassl, B.; Rowenczyk, L.; Tufenkji, N.; Feng, S.; Wiesner, M. Nanoplastics are neither microplastics nor engineered nanoparticles. *Nat. Nanotechnol.* **2021**, *16* (5), 501–507.
- (25) Pilechi, A.; Mohammadian, A.; Murphy, E. A numerical framework for modeling fate and transport of microplastics in inland and coastal waters. *Mar. Pollut. Bull.* **2022**, *184*, No. 114119.
- (26) Uzun, P.; Farazande, S.; Guven, B. Mathematical modeling of microplastic abundance, distribution, and transport in water environments: A review. *Chemosphere* **2022**, *288* (2), No. 132517.
- (27) Besseling, E.; Quik, J. T. K.; Sun, M.; Koelmans, A. A. Fate of nano- and microplastic in freshwater systems: A modeling study. *Environ. Pollut.* **2017**, *220*, 540–548.
- (28) Wang, Z.; Pilechi, A.; Fok Cheung, M.; Ariya, P. A. In-situ and real-time nano/microplastic coatings and dynamics in water using nano-DIHM: A novel capability for the plastic life cycle research. *Water Res.* **2023**, *235*, No. 119898.
- (29) United Nations Environment Programme *From pollution to solution: A global assessment of marine litter and plastic pollution*. UNEP Report, 2021. ISBN: 978-92-807-3881-0.
- (30) United Nations Environment Programme, *Inside the clean seas campaign against microplastics*. New, Stories & Speeches, 2022. <https://www.unep.org/news-and-stories/story/inside-clean-seas-campaign-against-microplastics>.
- (31) Pal, D.; Nazarenko, Y.; Preston, T. C.; Ariya, P. A. Advancing the science of dynamic airborne nanosized particles using Nano-DIHM. *Commun. Chem.* **2021**, *4* (1), 170.
- (32) Hall, R.; Pal, D.; Ariya, P. A. Novel dynamic technique, Nano-DIHM, for rapid detection of oil, heavy metals, and biological spills in aquatic systems. *Anal. Chem.* **2022**, *94* (32), 11390–11400.
- (33) Garcia-Sucerquia, J.; Xu, W.; Jericho, S. K.; Klages, P.; Jericho, M. H.; Kreuzer, H. J. Digital in-line holographic microscopy. *Appl. Opt.* **2006**, *45* (5), 836–850.
- (34) Xu, W.; Jericho, M. H.; Meinertzhausen, I. A.; Kreuzer, H. J. Digital in-line holography of microspheres. *Appl. Opt.* **2002**, *41* (25), 5367–5375.
- (35) Pal, D.; Amyot, M.; Liang, C.; Ariya, P. A. Real-time 4D tracking of airborne virus-laden droplets and aerosols. *Commun. Eng.* **2023**, *2* (1), 41.
- (36) Helm, J. M.; Swiergosz, A. M.; Haeberle, H. S.; Karnuta, J. M.; Schaffer, J. L.; Krebs, V. E.; Spitzer, A. I.; Ramkumar, P. N. Machine learning and artificial intelligence: Definitions, applications, and future directions. *Current Reviews in Musculoskeletal Medicine* **2020**, *13* (1), 69–76.
- (37) Soori, M.; Arezoo, B.; Dastres, R. Artificial intelligence, machine learning and deep learning in advanced robotics, a review. *Cognitive Robotics* **2023**, *3*, 54–70.
- (38) *4Deep in water imaging, Stingray Software User Guide*. Version 2.2.0, 2018.
- (39) Walcutt, N. L., An assessment of holographic microscopy for quantifying marine particle size and concentration. University of Rhode Island. Open Access Master's Theses, 2018. 1328.
- (40) Walcutt, N. L.; Knorlein, B.; Cetinic, I.; Ljubetic, Z.; Bosak, S.; Sgouros, T.; Montalbano, A. L.; Neeley, A.; Menden-Deuer, S.; Omand, M. M. Assessment of holographic microscopy for quantifying marine particle size and concentration. *Limnology and Oceanography: Methods* **2020**, *18* (9), 516–530.
- (41) Babajamaaty, G., Numerical simulation of microplastics transport in a part of Fraser River and detection of accumulation zones based on clustering methods. University of Ottawa. MSc Thesis, 2023.
- (42) Hervouet, J. M. *Parameter estimation. Hydrodynamics of free surface flows: modelling with the finite element method*; John Wiley & Sons, 2007. Chapter 9, 257–280.
- (43) Abramowitz, M.; Spring, K. R.; Keller, H. E.; Davidson, M. W. Basic principles of microscope objectives. *BioTechniques* **2002**, *33* (4), 772.
- (44) Keolmans, A. A.; Besseling, E.; Shim, W. J., Nanoplastics in the aquatic environment. Critical review. In *Marine Anthropogenic Litter*; Springer: Cham, 2015. Microplastics, 325–340.
- (45) Yu, S.; Shen, M.; Li, S.; Fu, Y.; Zhang, D.; Liu, H.; Liu, J. Aggregation kinetics of different surface-modified polystyrene nanoparticles in monovalent and divalent electrolytes. *Environ. Pollut.* **2019**, *255* (2), No. 113302.
- (46) Thoma, S. L. J.; Krauss, S. W.; Eckardt, M.; Chater, P.; Zobel, M. Atomic insight into hydration shells around faceted nanoparticles. *Nat. Commun.* **2019**, *10* (1), 995.
- (47) Mariano, S.; Tacconi, S.; Fidaleo, M.; Rossi, M.; Dini, L. Micro and nanoplastics identification: Classic methods and innovative detection techniques. *Frontiers in Toxicology* **2021**, *3*, No. 636640.
- (48) Jaferzadeh, K.; Fevens, T. HoloPhaseNet: fully automated deep-learning-based hologram reconstruction using a conditional generative adversarial model. *Biomedical Optics Express* **2022**, *13* (7), 4032–4046.
- (49) Hufnagl, B.; Steiner, D.; Renner, E.; Löder, M. G. J.; Laforsch, C.; Lohninger, H. A methodology for the fast identification and

- monitoring of microplastics in environmental samples using random decision forest classifiers. *Analytical Methods* **2019**, *11* (17), 2277–2285.
- (50) Davies, E. J.; Buscombe, D.; Graham, G. W.; Nimmo-Smith, W. A. M. Evaluating unsupervised methods to size and classify suspended particles using digital in-line holography. *Journal of Atmospheric and Oceanic Technology* **2015**, *32* (6), 1241–1256.
- (51) Bochdansky, A. B.; Jericho, M. H.; Herndl, G. J. Development and deployment of a point-source digital inline holographic microscope for the study of plankton and particles to a depth of 6000 m. *Limnology and Oceanography: Methods* **2013**, *11* (1), 28–40.
- (52) Henneberger, J.; Fugal, J. P.; Stetzer, O.; Lohmann, U. HOLIMO II: a digital holographic instrument for ground-based in situ observations of microphysical properties of mixed-phase clouds. *Atmospheric Measurement Techniques* **2013**, *6* (11), 2975–2987.
- (53) Zhu, Y.; Lo, H. K. A.; Yeung, C. H.; Lam, E. Y. Microplastic pollution assessment with digital holography and zero-shot learning. *APL Photonics* **2022**, *7* (7), No. 066103.
- (54) Zhu, Y.; Hang Yeung, C.; Lam, E. Y. Microplastic pollution monitoring with holographic classification and deep learning. *Journal of Physics: Photonics* **2021**, *3* (2), No. 024013.
- (55) Nguyen, B.; Claveau-Mallet, D.; Hernandez, L. M.; Xu, E. G.; Farner, J. M.; Tufenkji, N. Separation and analysis of microplastics and nanoplastics in complex environmental samples. *Acc. Chem. Res.* **2019**, *52* (4), 858–866.
- (56) Zhang, W.; Wang, Q.; Chen, H. Challenges in characterization of nanoplastics in the environment. *Front. Environ. Sci. Eng.* **2021**, *16* (1), 11.
- (57) Patil, S. M.; Rane, N. R.; Bankole, P. O.; Krishnaiah, P.; Ahn, Y.; Park, Y.; Yadav, K. K.; Amin, M. A.; Jeon, B. An assessment of micro- and nanoplastics in the biosphere: A review of detection, monitoring, and remediation technology. *Chemical Engineering Journal* **2022**, *430*, No. 132913.
- (58) Chen, G.; Li, Y.; Wang, J. Occurrence and ecological impact of microplastics in aquaculture ecosystems. *Chemosphere* **2021**, *274*, No. 129989.
- (59) Li, C.; Jiang, B.; Guo, J.; Sun, C.; Shi, C.; Huang, S.; Liu, W.; Wu, C.; Zhang, Y. Aging process of microplastics in the aquatic environments: Aging pathway, characteristic change, compound effect, and environmentally persistent free radicals formation. *Water* **2022**, *14* (21), 3515.
- (60) He, W.; Liu, S.; Zhang, W.; Yi, K.; Zhang, C.; Pang, H.; Huang, D.; Huang, J.; Li, X. Recent advances on microplastic aging: Identification, mechanism, influence factors, and additives release. *Sci. Total Environ.* **2023**, *889*, No. 164035.
- (61) Hao, Z.; Li, W.; Hou, B.; Su, P.; Ma, J. Characterization method for particle extraction from raw-reconstructed images using U-net. *Frontiers in Physics* **2022**, *9*, No. 816158.
- (62) Saharia, C.; Ho, J.; Chan, W.; Salimans, T.; Fleet, D. J.; Norouzi, M. Image super-resolution via iterative refinement. In *IEEE Transactions on Pattern Analysis and Machine Intelligence* **2023**, *45*, 4 4713–4726 IEEE.
- (63) Jericho, M. H.; Kreuzer, H. J.; Kanka, M.; Riesenber, R. Quantitative phase and refractive index measurements with point-source digital in-line holographic microscopy. *Appl. Opt.* **2012**, *51* (10), 1503–1515.
- (64) Ravasio, C.; Cremonesi, L.; Artoni, C.; Delmonte, B.; Maggi, V.; Potenza, M. A. C. Optical characterization of mineral dust from the EAIST project with digital holography. *ACS Earth and Space Chemistry* **2021**, *5* (10), 2855–2864.
- (65) Li, J.; Guala, M.; Hong, J. Snow particle analyzer for simultaneous measurements of snow density and morphology. *JGR Atmos.* **2023**, *128* (16), No. e2023JD038987.
- (66) Bai, Y.; Xu, L.; He, C.; Zhu, L.; Yang, X.; Jiang, T.; Nie, J.; Zhong, W.; Wang, Z. L. High-performance triboelectric nanogenerators for self-powered, in-situ and real-time water quality mapping. *Nano Energy* **2019**, *66*, No. 104117.
- (67) Leigh, C.; Alsibai, O.; Hyndman, R. J.; Kandanaarachchi, S.; King, O. C.; McGree, J. M.; Neelamraju, C.; Strauss, J.; Talagala, P.; Turner, R. D. R.; Mengersen, K.; Peterson, E. E. A framework for automated anomaly detection in high frequency water-quality data from in situ sensors. *Science of The Total Environment* **2019**, *664*, 885–898.
- (68) Alam, A. U.; Clyne, D.; Jin, H.; Hu, N. X.; Deen, M. J. Fully integrated, simple, and low-cost electrochemical sensor array for in situ water quality monitoring. *ACS Sensors* **2020**, *5* (2), 412–422.
- (69) Quinn, N. W. T.; Ortega, R.; Rahilly, P. J. A.; Royer, C. W. Use of environmental sensors and sensor networks to develop water and salinity budgets for seasonal wetland real-time water quality management. *Environmental Modelling & Software* **2010**, *25* (9), 1045–1058.
- (70) Kim, J.; Yu, J.; Kang, C.; Ryang, G.; Wei, Y.; Wang, X. A novel hybrid water quality forecast model based on real-time data decomposition and error correction. *Process Safety and Environmental Protection* **2022**, *162*, 553–565.
- (71) Mofijur, M.; Ahmed, S. F.; Rahman, S. M. A.; Arafat Siddiki, S. Y.; Islam, A.; Shahabuddin, M.; Ong, H. C.; Mahlia, T. M. I.; Djavanroodi, F.; Show, P. L. Source, distribution and emerging threat of micro- and nanoplastics to marine organism and human health: Socio-economic impact and management strategies. *Environmental Research* **2021**, *195*, No. 110857.
- (72) Sarkar, B.; Dissanayake, P. D.; Bolan, N. S.; Dar, J. Y.; Kumar, M.; Haque, M. N.; Mukhopadhyay, R.; Ramanayaka, S.; Biswas, J. K.; Tsang, D. C. W.; Rinklebe, J.; Ok, Y. S. Challenges and opportunities in sustainable management of microplastics and nanoplastics in the environment. *Environ. Res.* **2022**, *207*, No. 112179.
- (73) Zhang, B.; Chao, J.; Chen, L.; Liu, L.; Yang, X.; Wang, Q. Research progress of nanoplastics in freshwater. *Science of The Total Environment* **2021**, *757*, No. 143791.
- (74) Blevins, M. G.; Allen, H. L.; Colson, B. C.; Cook, A. M.; Greenbaum, A. Z.; Hemami, S. S.; Hollmann, J.; Kim, E.; LaRocca, A. A.; Markoski, K. A.; Miraglia, P.; Mott, V. L.; Robberson, W. M.; Santos, J. A.; Sprachman, M. M.; Swierk, P.; Tate, S.; Witinski, M. F.; Kratchman, L. B.; Michel, A. P. M. Field-portable microplastic sensing in aqueous environments: A perspective on emerging techniques. *Sensors* **2021**, *21* (10), 3532.
- (75) Glasgow, H. B.; Burkholder, J. M.; Reed, R. E.; Lewitus, A. J.; Kleinman, J. E. Real-time remote monitoring of water quality: a review of current applications, and advancements in sensor, telemetry, and computing technologies. *Journal of Experimental Marine Biology and Ecology* **2004**, *300* (1–2), 409–448.
- (76) Lakshmikantha, V.; Hiriyanagowda, A.; Manjunath, A.; Patted, A.; Basavaiah, J.; Anthony, A. A. IoT based smart water quality monitoring system. *Global Transitions Proceedings* **2021**, *2* (2), 181–186.
- (77) Calore, D.; Fraticelli, N. State of the art offshore in situ monitoring of microplastic. *Microplastics* **2022**, *1* (4), 640–650.
- (78) Fu, X.; Shang, X.; Sun, X.; Yu, H.; Song, M.; Chang, C. Underwater hyperspectral target detection with band selection. *Remote Sensing* **2020**, *12* (7), 1056.
- (79) Picheral, M.; Catalano, C.; Brousseau, D.; Claustre, H.; Coppola, L.; Leymarie, E.; Coindat, J.; Dias, F.; Fevre, S.; Guidi, L.; Irisson, J. O.; Legendre, L.; Lombard, F.; Mortier, L.; Penkerch, C.; Rogge, A.; Schmechtig, C.; Thibault, S.; Tixier, T.; Waite, A.; Stemmann, L. The underwater vision profiler 6: an imaging sensor of particle size spectra and plankton, for autonomous and cabled platforms. *Limnology and Oceanography: Methods* **2022**, *20* (2), 115–129.
- (80) Han, J.; Shoeiby, M.; Malthus, T.; Botha, E.; Anstee, J.; Anwar, S.; Wei, R.; Armin, M. A.; Li, H.; Petersson, L. Underwater image restoration via contrastive learning and a real-world dataset. *Remote Sensing* **2022**, *14* (17), 4297.